Current Photovoltaic Research 11(1) 8-12 (2023)
DOI:https://doi.org/10.21218/CPR.2023.11.1.008
pISSN 2288-3274
eISSN 2508-125X

Effect of Ag Alloying on Device Performance of Flexible CIGSe Thin-film Solar Cells Using Stainless Steel Substrates

Awet Mana Amare[1] · Inchan Hwang[1] · Inyoung Jeong[1] · Joo Hyung Park[1] · Jin Gi An[1] · Soomin Song[1] · Young-Joo Eo[1] · Ara Cho[1] · Jun-Sik Cho[1] · Seung Kyu Ahn[1] · Jinsu Yoo[1] · SeJin Ahn[1] · Jihye Gwak[1] · Hyun-wook Park[2] · Jae Ho Yun[2] · Kihwan Kim[1]* · Donghyeop Shin[1]*

[1]Photovoltaics Research Department, Korea Institute of Energy Research (KIER), 152-Gajeong-ro, Yuseong-gu, Daejeon, 34129, Korea
[2]Department of Energy Engineering, Korea Institute of Energy Technology, Naju, 58217, Korea

Received February 10, 2023; Revised March 20, 2023; Accepted March 20, 2023

ABSTRACT: In this work, we investigated the thickness of Ag precursor layer to improve the performance of flexible CIGSe solar cells grown on stainless steel (STS) substrates through three-stage co-evaporation with Ga grading followed by alkali treatments. The small amount of incorporated Ag in CIGSe films showed enhancement in the grain size and device efficiency. With an optimal 6 nm-thick Ag layer, the best cell on the STS substrate yielded more than 16%, which is comparable to the soda-lime glass (SLG) substrate. Thus, the addition of controlled Ag combined with alkali post-deposition treatment (PDT) led to increased open-circuit voltage (V_{OC}), accompanied by the increased built-in potential as confirmed by capacitance-voltage (C-V) measurements. It is related to a reduction of charge recombination at the depletion region. The results suggest that Ag alloying and alkali PDT are essential for producing highly efficient flexible CIGSe solar cells.

Key words: Flexible solar cells, Stainless steel substrate, Ag alloying, Alkali post-deposition treatment

1. Introduction

Polycrystalline Cu(In,Ga)Se_2 (CIGSe) absorber is one of the most promising photovoltaic materials, as their cell efficiency has steadily increased up to 23.35% on glass[1]. However, its rigid soda-lime glass (SLG) substrate limits its use on curved building and automobile applications. Therefore, alternative substrates have been utilized for flexible CIGSe solar cells. Several groups have achieved high efficiencies of flexible CIGSe solar cells with 21.4%[2] and 20.56%[3] for polyimide (PI) and stainless steel (STS) substrates, respectively.

In order to enhance the device performance, high-quality of CIGSe films should be obtained, and detrimental defects also need to be sufficiently suppressed. In this regard, CIGSe films have been grown by a three-stage process while the Ga grading in CIGSe films is controlled in terms of bandgap engineering. Then, it provides an improved band alignment and reduced recombination at interfaces, thereby improving the collection of photo-generated minority carriers[4, 5]. In addition, alkali doping for CIGSe films has been widely applied to suppress harmful defects. Specifically, post-deposition treatment (PDT) method was adopted by supplying various alkali compounds including Na, K, Rb, and Cs[6, 7]. However, as mentioned, to realize flexible solar cells, CIGSe films should be grown on flexible PI and STS substrates which are different from conventional SLG substrates. As a result, the deposition conditions for high-quality CIGSe film growth should be investigated based on the substrate material properties such as thermal and mechanical properties.

In this work, flexible CIGSe solar cells were fabricated on an STS substrate since its substrate has no limitation in process temperature compared with PI. However, Fe, i.e., a constituent element is known as a killer ion to form deep defect levels in CIGSe bulk, so that suitable process temperature which does not accelerate Fe diffusion needs to be found while employing a diffusion barrier. Moreover, the STS surface roughness is relatively high. It means that CIGSe film quality can be dependent on the STS surface. To overcome such unfavorable growth conditions, the introduction of Ag in the CIGSe film was considered. In general, low-melting-point Ag reduces crystallization temperature and alloying a small amount of Ag induces a negligible change in band gap[8, 9]. This leads to improved cry-

*Corresponding author: kimkh@kier.re.kr (Kihwan Kim);
donghyeop.shin@kier.re.kr (Donghyeop Shin)

stallization and surface morphology, resulting in better film quality of the CIGSe films[10]. Herein, the optimal Ag content to grow high-quality CIGSe films has been investigated. When it comes to control over defect passivation, alkali PDT is known as the most effective way to improve defect properties of CIGSe films. Thus, heavy alkali RbF PDT combined with NaF PDT was introduced immediately after CIGSe film growth.

Consequently, when the 6 nm Ag was included in the film, the grain size of CIGSe became larger. In addition, the optimized alkali PDT conditions resulted in an improvement in device efficiency. The best cell on the STS substrate yielded more than 16% efficiency, comparable to the cell on an SLG substrate. It suggests that the Ag alloying combined with alkali PDT is essential to make high-efficiency flexible CIGSe solar cells.

2. Experimental method

100 μm-thick stainless steel foil (430 series) was used as a substrate. On top of the STS, 200 nm-thick Cr layer served as a diffusion layer to minimize Fe diffusion from STS substrate during high-temperature process. Then, ~800 nm-thick Mo back contacts were deposited onto clean STS substrates using DC magnetron sputtering method. To find an optimal Ag content in CIGSe films, the Ag layer thickness was adjusted from 2 to 15 nm by using a thermal evaporator. Next, CIGSe absorbers were deposited on STS substrates using a three-stage co-evaporation process followed by NaF and RbF PDT. The thickness of CIGSe films is approximately 2.0 μm showing a nominal composition of [Cu]/([In]+[Ga]) ~ 0.9 and [Ga]/([In]+[Ga]) ~ 0.34. Details on CIGSe film growth is shown in Figure 1. 60 nm-thick CdS films were prepared by a chemical bath deposition (CBD) method. Then, 50 nm-thick i-ZnO and 150 nm-thick indium tin oxide (ITO) films were sequentially deposited by RF sputtering method. Finally, 1 μm-thick aluminum grids as a front electrode were deposited using thermal evaporation. The structure of a

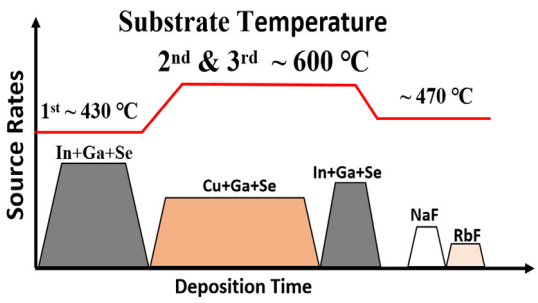

Fig. 1. Three-stage process for CIGSe film growth

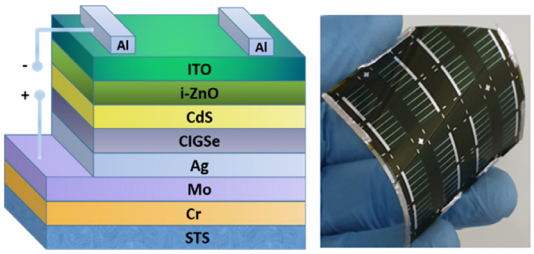

Fig. 2. Device structure of flexible CIGS solar cells on a STS substrate

flexible CIGSe solar cell on the STS is schematically displayed in Figure 2.

To characterize the properties of CIGSe films, scanning electron microscopy (SEM) and energy-dispersive spectroscopy (EDS) measurements were carried out using S-4800 (HITACHI, Japan). Light current density-voltage (J-V) curves were measured under standard test conditions (AM 1.5G at 25°C) using McScience solar simulator. External quantum efficiency (EQE) spectra were measured by McScience K3100. The capacitance-voltage (C-V) profiles were recorded using an Agilent-4284 Precision LCR meter at 100 kHz in the dark condition.

3. Result and discussion

Figure 3 shows SEM images of the plain and cross-sectional views of CIGSe films grown on STS and SLG substrates. When a small amount of Ag was incorporated in the CIGSe film by preparing the Ag layer on top of Mo back contact, the grain sizes of CIGSe became bigger compared to CIGSe grains without Ag alloying. Especially, the Ag-alloyed grains extended throughout the film which is desirable in terms of charge carrier separation without recombination. According to literature, Ag alloying lowers a eutectic point to form CIGSe film, facilitating an improved intermixing of constituent elements, thereby increasing CIGSe grain sizes[8, 9].

To find the optimal amount of Ag layer in the film, the thickness of Ag layer was adjusted from 2 to 15 nm as shown in Figure 4. The best efficiency of CIGSe cell was obtained from a 6 nm Ag layer. When the Ag amount was increased, the photovoltaic parameters were degraded. The open-circuit voltage and short-circuit current were seriously lowered, thereby decreasing the device performance. The decrease in PV parameters could be possibly caused by compositional non-uniformity on the CIGSe surface when Ag alloying content is increased in the CIGSe film. Some literature has already reported that segregation

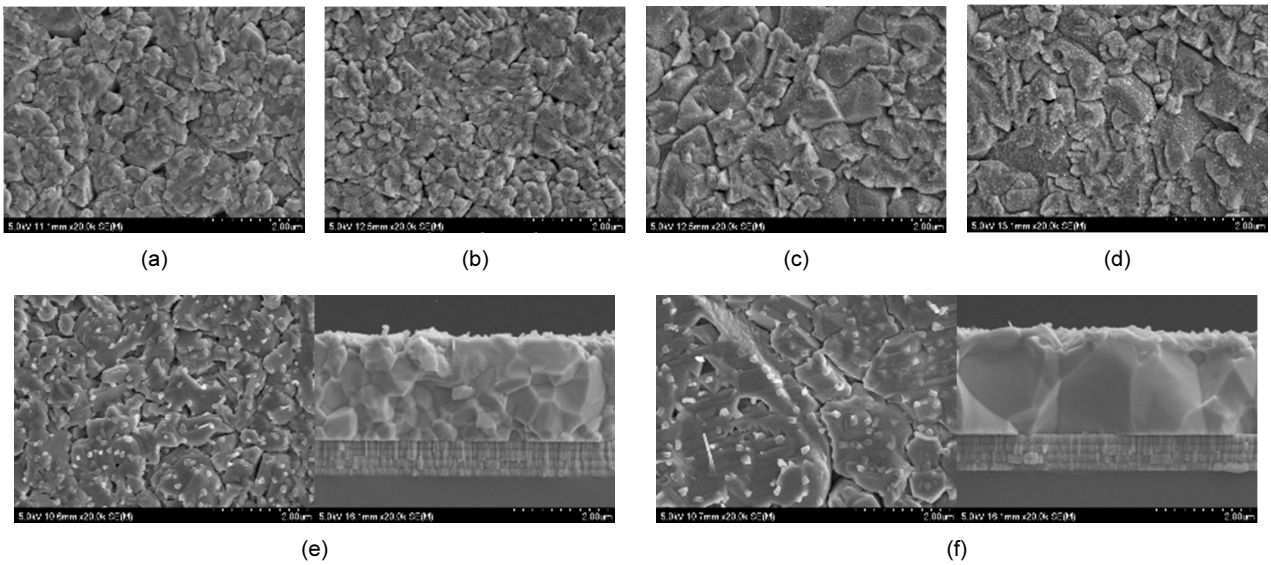

Fig. 3. Plain and cross-sectional SEM images of CIGSe films on STS and SLG substrates: (a) STS without Ag and alkali PDTs, (b) STS with the only Na PDT only without Ag doping, (c) STS with 6 nm Ag doping and Na PDT and (d) STS with 6 nm Ag doping and Na/Rb PDTs. As a purpose to probe effect of Ag alloying on the CIGS microstructure, (e) SLG with Na/Rb PDTs and (f) SLG with 6 nm Ag doping and Na/Rb PDTs.

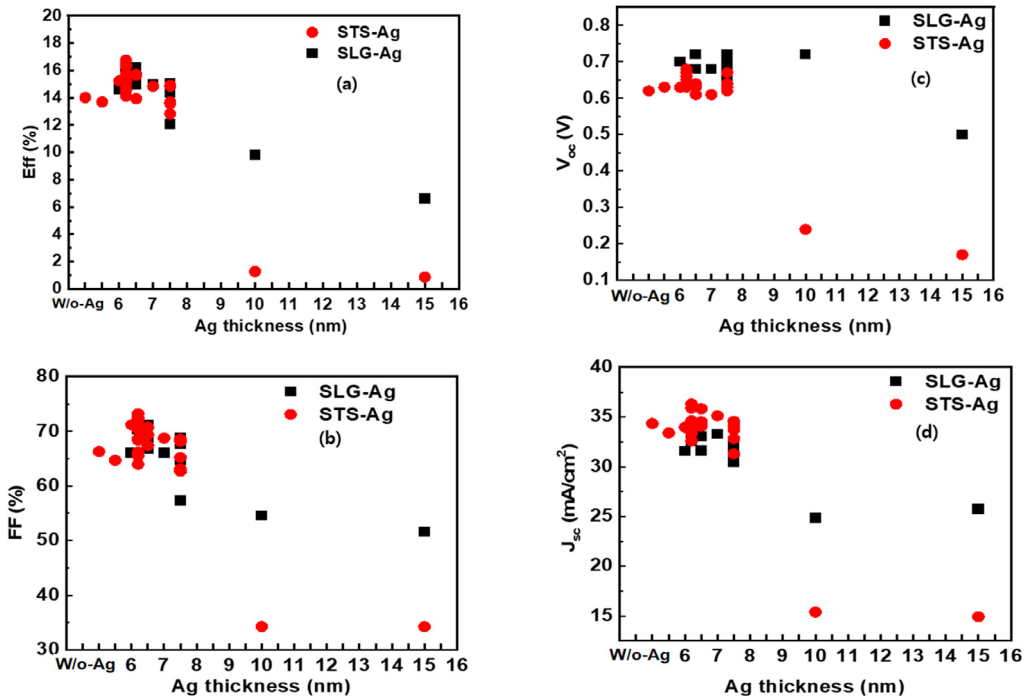

Fig. 4. Photovoltaic parameters of CIGSe solar cells on STS and SLG substrates as a function of Ag layer thickness.(a) efficiency (Eff), (b) Fill-factor (FF), (c) open-circuit voltage (V_{OC}), and (d) short-circuit density (J_{sc}).

of secondary phases could result from uncontrolled Ag alloying, typically at the CIGSe surface[11, 12]. Thus, the performance of solar cells might be adversely affected by the relatively high amount of Ag by secondary phases[11, 12]. Despite such a small amount, it is essential to note that Ag plays a significant role in improving the microstructure of CIGSe films.

In addition to optimization of Ag inclusion, NaF and RbF PDT processes were optimized by adjusting the evaporation temperature of NaF and RbF sources. First of all, as shown in Figure 5, the NaF source temperature was changed from 660 to 690°C. As a result, the cell efficiencies were centered at 670°C which is an optimal condition for NaF PDT. At the RbF source temperature of 480°C, the best efficiencies were shown up to more than 16%. Given this observed results, the process window

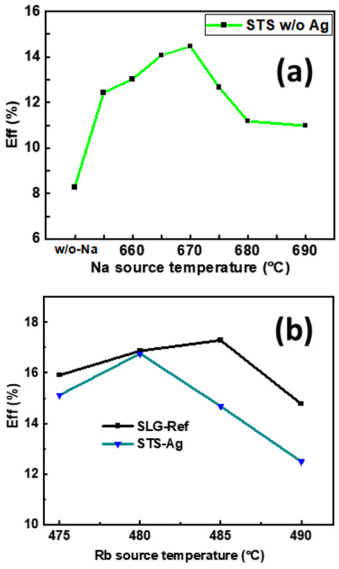

Fig. 5. Optimization of (a) NaF and (b) RbF PDT processes by adjusting the alkali source evaporation temperatures

of PDT process seems to be relatively narrow. Nevertheless, the optimized condition shows reproducible results.

As shown in Table 1, the photovoltaic parameters are summarized according to the optimization of Ag alloying and alkali PDT. Basically, the STS cell without the abovementioned processes yielded less than 10% with a low open circuit voltage (V_{OC}) of 0.56 V. First, Na doping induced significant enhancement in the device efficiency from 8 to 14%. The improvement in V_{OC} contributed to increased device efficiency. It indicates that only Na doping seems to suppress detrimental defects. When Ag was introduced, there was an additional increase in device efficiency. Finally, the best cell on STS with heavy alkali RbF PDT showed higher efficiency of 16.7%, which is about 0.6% lower compared to the efficiency of the reference cell on SLG, which is 17.29% efficiency.

Figure 6 shows C-V measurements plotted as $1/C^2$-V to determine the carrier concentration and built-in potential in the CIGSe solar cells for three devices, including STS-Na, STS-Na-Ag, and STS-Na-Ag-Rb. The net carrier concentrations for the devices determined at 0 V are 2.4 x10^{15}, 2.6 x10^{15}, and 3.6 x10^{15} cm^{-3} for STS-Na, STS-Na-Ag, and STS-Na-Ag-Rb CIGSe solar cells respectively. There is no significant change in carrier density for the three devices. However, the best cell with optimal Ag alloying combined with alkali PDT has gained improved built-in potential, as indicated for each device in Fig. 6. A higher built-in potential represents a stronger electric field and reduction in charge recombination at the depletion region, which is associated with increased V_{OC} and resultant device efficiency.

Table 1. Summary of photovoltaic parameters for flexible CIGSe solar cells depending on optimal Ag alloying and NaF/RbF PDT processes

Substrate type and Samples Name	Ag	PDT	Effi. (%)	Voc (V)	Jsc (mA/cm²)	FF (%)
SLG-Ref	x	Na&Rb	17.29	0.69	33.99	73.71
STS	x	X	8.28	0.56	29.96	49.22
STS-Na	x	Na	14.02	0.62	34.35	66.32
STS-Na-Ag	o	Na	15.65	0.63	35.83	69.34
STS-Na-Ag-Rb	o	Na&Rb	16.76	0.66	35.90	70.37

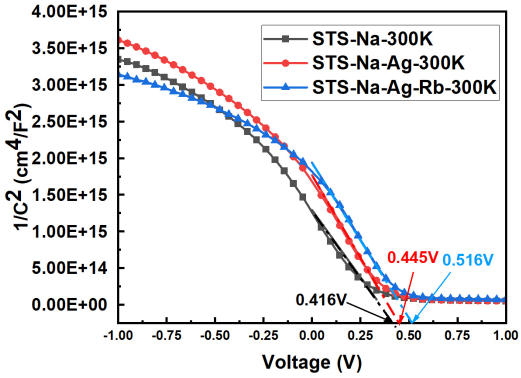

Fig. 6. Plot of $1/C^2$ versus applied bias V for CIGSe solar cells on an STS substrate

Although we expect the built-in potential to be greater than the devices' open-circuit voltage, the extrapolated voltages are smaller than the open-circuit voltages of the STS-Na, STS-Na-Ag, and STS-Na-Ag-Rb devices shown in Table 1. This is because measurements of doping concentration and built-in potential in crystalline materials with a homojunction may be easily accomplished using capacitance-voltage (C-V) measurements. However, interpreting and extracting experimental data for thin film devices with multilayer interfaces and heterojunctions is challenging[13]. As a result, capacitance can be contributed by numerous layers and interfaces[14, 15]. This may explain why Figure 6 exhibits a voltage axis intercept greater than 100 mV lower than the device's open-circuit voltage. However, having observed the trend in the built-in potential increase in Figure 6, the plot could indicate device quality improvements by combining Ag precursor and Alkali PDT doping. Moreover, The inverse square of the capacitance ($1/C^2$) plot against the voltage for the RbF alkali-doped device intersects with the other graphs at reverse bias voltages. As can be observed from the plot, the graph begins to flatten at small reverse bias voltage, which indicates the decrease of the $1/C^2$ slope for the RbF doped device. Therefore, as the doping concentration is inversely

related to the slope, the doping concentration will increase in the reverse bias. Thus, the alkali RbF doping seems to affect the doping concentration in this device.

4. Conclusions

In this work, Ag precursor layer thickness was tuned from 2 to 15 nm to fabricate high-efficiency flexible CIGSe solar cells grown on stainless steel (STS) foil. Furthermore, the addition of Na and Rb alkali elements was optimized by varying source temperatures to enhance the performance of CIGSe solar cells. As a result, an optimal 6 nm Ag precursor layer incorporated into CIGSe film improved the CIGSe grain size as well as the cross-sectional microstructure. The optimized alkali PDT conditions, along with the optimal Ag layer, induced improvement in device efficiency. The best cell on the STS substrate yielded more than 16%, which is higher than the cell on the SLG substrate. Interestingly, as we demonstrated by capacitance-voltage measurements, Ag alloying improved carrier collection, increasing built-in potential. Therefore, the combined optimization of Ag alloying and alkali PDT plays crucial role in the fabrication of high-efficiency CIGSe solar cells on flexible substrates.

Acknowledgments

This research was financially supported by the Korea Institute of Energy Research (KIER) (grant no. C3-2401, 2402, 2403) and the National Research Foundation (grant no. 2022M3J1A1063019) funded by the Ministry of Science and ICT.

References

1. Nakamura, M., et al., "Cd-free Cu(In,Ga)(Se,S)$_2$ thin-film solar cell with record efficiency of 23.35%," IEEE Journal of Photovoltaics, 9(6), 863-1867 (2019).
2. Empa, "21.4% record efficiency for flexible solar cells," 2021, [cited 2023-03-10]; Available from: https://www.empa.ch/web/s604/cigs-efficiency-record-2021
3. MiaSole', "New World Record Efficiency with Flexible CIGS Solar Cell," 2019[cited 2023-02-04]; Available from: https://miasole.com/new-world-record-efficiency-with-flexible-cigs-solar-cell/.
4. Gloeckler, M. and J.Sites, "Band-gap grading in Cu(In,Ga)Se$_2$ solar cells," Journal of Physics and Chemistry of Solids, 66(11), 1891-1894 (2005).
5. Aboulfadl, H., et al., "Alkali Dispersion in (Ag,Cu)(In,Ga)Se$_2$ Thin Film Solar Cells—Insight from Theory and Experiment," ACS applied materials & interfaces, 13(6), 7188-7199 (2021).
6. Muzzillo, C.P., H.M. Tong, and T. Anderson, "Chemistry of K in Cu(In,Ga)Se$_2$ photovoltaic absorbers: effects of temperature on Cu-K-In-Se films," Journal of Alloys and Compounds, 726, 538-546 (2017).
7. Khatri, I., et al., "Effect of potassium fluoride post-deposition treatment on Cu(In,Ga)Se$_2$ thin films and solar cells fabricated onto soda lime glass substrates," Solar Energy Materials and Solar Cells, 155, 280-287 (2016).
8. Kim, K., et al., "Ag incorporation in low-temperature grown Cu(In,Ga)Se$_2$ solar cells using Ag precursor layers," Solar Energy Materials and Solar Cells, 146, 114-120 (2016).
9. Kim, G., et al., "Thin Ag precursor layer-assisted co-evaporation process for low-temperature growth of Cu(In,Ga)Se$_2$ thin film," ACS applied materials & interfaces, 11(35), 31923-31933 (2019).
10. Wang, Y., S. Lv, and Z. Li, "Review on incorporation of alkali elements and their effects in Cu(In,Ga)Se$_2$ solar cells," Journal of Materials Science & Technology, 96, 179-189 (2022).
11. Simchi, H., et al., "An Investigation of the Surface Properties of (Ag,Cu)(In,Ga)Se$_2$ Thin Films," IEEE Journal of Photovoltaics, 2(4), 519-523 (2012).
12. Kim, K., et al., "Highly efficient Ag-alloyed Cu(In,Ga)Se$_2$ solar cells with wide bandgaps and their application to chalcopyrite-based tandem solar cells," Nano Energy, 48, 345-352 (2018).
13. Heath, J. and P. Zabierowski, "Capacitance spectroscopy of thin-film solar cells," Advanced characterization techniques for thin-film solar cells", 81-105 (2011).
14. Yu, H.J., et al., "Light-soaking effects and capacitance profiling in Cu(In,Ga)Se$_2$ thin-film solar cells with chemical-bath-deposited ZnS buffer layers," Physical Chemistry Chemical Physics, 18(48), 33211-33217 (2016).
15. Babbe, F., et al., "Potassium fluoride postdeposition treatment with etching step on both Cu-rich and Cu-poor CuInSe$_2$ thin film solar cells," Physical Review Materials, 2(10), 105405 (2018).